Publishing House
AKAPIT

COMPUTER METHODS IN MATERIALS SCIENCE

Informatyka w Technologii Materiałów

Vol. 7, 2007, No. 4

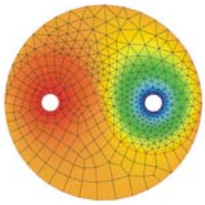

MAPPING MICROSTRUCTURE IN AC AND PSC TESTPIECES DEFORMED AT HIGH TEMPERATURE

BRYAN ROEBUCK[1], KEN P MINGARD[1], MATTHEW BROOKS[1], ERIC J PALMIERE[2], BRAD P WYNNE[2], MATTHEW J THOMAS[2]

[1]NPL, Teddington, Middlesex, London, UK
[2]IMMPETUS, Institute for Microstructural and Mechanical Process Engineering,
The University of Sheffield, Sheffield, UK
Corresponding author: bryan.roebuck@npl.co.uk (B. Roebuck)

Abstract

Good measurement infrastructure is vital for providing essential data for process model development that is used to provide better control during production. Recently a consortium of research technology organisations within the UK have developed "good practice guides" for hot deformation tests, such as axisymmetric compression, plane strain compression and solid torsion. Taking this activity forward a key objective now is to develop a "Good Practice Guide" for measuring the local microstructures in terms of grain and phase size, shape, spatial distribution and volume fraction of second phase (or recrystallised fraction). Measurement issues are being addressed with new characterisation methods, for example, orientation and hardness mapping, predominantly in these representative hot deformation compression tests.

Key words: microstructure mapping, hot compression tests, structure characterisation

1. INTRODUCTION

Industry needs a better understanding of how microstructures develop during processing in order to develop appropriate process models, because trial-and-error methods are no longer viable. Competition is moving the forging and the wider metals processing industry towards higher integrity, higher value components with reduced levels of scrap and wastage. Lower process costs through improved process models will bring benefits for energy consumption, reduced harmful emissions and less material wastage. In order to remain competitive against low cost producers the steel industry is driving towards the production of technologically demanding steel types and more accurately controlled processing. Whilst some technologies are very well established, others are newly emerging. Industry, academia and other research organisations are working towards good testing procedure (Roebuck et al, 2006; Loveday et al., 2006; Roebuck et al., 2006) in dynamic high temperature testing regimes. It is also important to produce guidelines for microstructural examination and to define local deformation conditions to compare computed and measured maps of microstructural evolution to provide information for the validation of appropriate models. A key requirement is the need to study local microstructures, and this has been conducted in the current work through microstructure mapping using predominantly orientation imaging (EBSD) and microhardness mapping.

Electron Back Scatter Diffraction, EBSD, is increasingly used as a tool for characterising the microstructure of a wide range of engineering materials by mapping the crystallographic orientation at many points across a polished section of a suitable test-

 ISSN 1641-8581

piece (Humphreys, 2001; Randle, 2003). The automated nature of EBSD means it can provide a large amount of information which is less susceptible to the skill and subjectivity of individual. However, there is still a need for care in specimen preparation and choice of operating and analysis conditions. Indexing rates of >85% are generally required for minimal errors but with suitable noise reduction to 'infill' non-indexed points this requirement for indexing can fall to about 50% (Humphreys, 2001). EBSD maps typically do not correctly identify 100% of the points examined, so the effects on measured grain size of post-acquisition methods to correct these points, or noise reduction, should also be considered. Thus, in formulating a guide for good practice in the metallographic characterisation of heterogeneity in structure from an EBSD perspective there are various issues that need to be considered; for example:

- Microscope Stage Drift
  An acceptable level of drift needs to be defined. Knowledge of stage drift is vital as it can introduce errors in length measurements, which further vary with changes in step size and diffraction pattern acquisition times.
- EBSD Software
  There are two major analytical software packages in use (hkl-Channel 5 and TSL) and questions arise as to the comparability of measurements using the different systems.
- Data interpretation and orientation indication
  How a grain is represented in misorientation space, in addition to the transparency of the software for microstructural mapping can give rise to systematic uncertainty.
- Size classification, by number or by area
- Grain size representation (mean linear intercept or equivalent circle diameter).
- Mapping large areas and how to quantify gradients in structure. For example, stitching mapped areas together, running averages, defining strips for quantification, selection of specific size classes and algorithms for initiating and defining EBSD mapping parameters.

Figure 1 shows an orientation map obtained using an electron backscattered diffraction (EBSD) technique (Humphreys, 2001; Randle, 2003) for a Ni superalloy (Waspaloy) with inverse pole figure colouring. The map was acquired with a 1 μm step size from the centre line of an axial cross section of a cylindrical axisymmetric compression sample. The sample was produced with a relatively high friction coefficient between sample and platens, with a strain rate of 0.01 s^{-1} at a temperature of 1040°C. The high friction results in a region of large unrecrystallised grains, evidenced by EBSD measurements of strain, close to the surface while the inner region consists of many smaller recrystallised grains. It is important to be able to quantify this heterogeneity in structure and define where in the testpiece is the optimum position for making measurements. In the current research the microstructure studies are largely being conducted by optical and EBSD measurements and these are complemented by the use of a scanning depth sensing microhardness test system recently developed at NPL (Roebuck et al., 2001).

In this study both microstructure and microhardness maps have been acquired from sections through test samples of uniaxially compressed cylinders or plane strain compression testpieces of a 316L stainless steel and a Ni superalloy, Waspaloy. The samples were compressed under dry non-lubricated conditions at strain rates of 1 s^{-1} and 0.01 s^{-1} at temperatures of 950 °C and 1040 °C for the 316L and Waspaloy respectively, to a total strain of 0.5. Following deformation the samples were immediately water quenched at an estimated cooling rate of 50 °C/s. A high strain rate combined with low friction gives rise to temperature inhomogeneities whereas high strain rate and high friction leads to both temperature and strain pattern heterogeneity. Details of the testing conditions are given in Table 1; three samples of each condition were generated for parallel examination at collaborating organisations.

Sections were cut and polished, using colloidal silica for 30 minutes as the final polishing stage and mapped by EBSD in a Cambridge 360 W-filament SEM operating at 15kV with a 1-3 nA probe current producing a spot size of approximately 0.15-

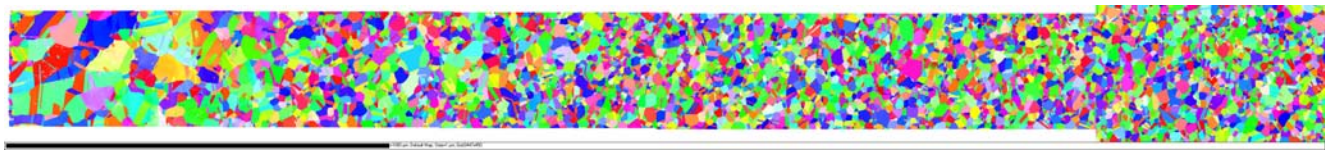

Fig. 1. *EBSD map of grain orientation in a section taken from a uniaxially compressed sample of Waspaloy. Top surface on left of map, centre of sample on right.*

0.25 μm. The EBSD patterns were acquired on a Nordlys detector using HKL software. The SEM magnification was calibrated with a square grid specimen, itself calibrated by a laser diffraction technique, and tilted at the same angle as the sample during EBSD mapping. After EBSD examination the 316L sample was electrolytically etched with 10% oxalic acid to reveal grain boundaries for light optical microscopy and linear intercept measurement of grain size.

Table 1. *Testing conditions*

Test number	Material	Initial temp. (°C)	Friction	Strain (s^{-1})
W1	Waspaloy	1040	lubricated	0.01
W2	Waspaloy	1040	dry	0.01
W3	Waspaloy	1040	lubricated	1
W4	Waspaloy	1040	dry	1
S1	316L	950	lubricated	0.01
S2	316L	950	dry	0.01
S3	316L	950	lubricated	1
S4	316L	950	dry	1

The scanning microhardness measurements were acquired using a new system developed at NPL (Roebuck et al., 2001). The system uses the principle of depth sensing hardness, allowing the measurement process to be fully automated. A diamond indenter is applied to the surface of the testpiece and hardness is calculated from the load and the indentation depth. A raster of indents can be placed by computer control to map the variation in hardness. Local mechanical property information can be rapidly obtained from a measurement of microindentation hardness. The NPL instrument, the SIMM, has been constructed with a relatively high speed facility to map large areas quickly. Typically an array of 100 × 100 indents takes about 10 h, i.e. about 4 s/indent. Force and displacement are monitored continuously during the complete indentation cycle. The machine currently operates in the micro to mesoscale range, 0.02-20 N, (approximately 2 gf-2 kgf), with a load resolution of 2 mN (0.2 gf) and a depth-sensing resolution of 20 nm, using a specially designed capacitance displacement sensor. The loading mechanism uses a piezoelectric actuator. A piezoelectric system has the potential to be quick, with a high resolution. However, the piezo actuator is limited to about ± 50 μm movement, so to allow coarse positioning the complete assembly is mounted on a high-precision motorised Z stage. The Z stage is driven to within a few micrometres of the surface, and the piezoelectric mechanism used to perform the indentation.

Conventional microhardness values are calculated using the standard Vickers formula

$$\mathrm{HV} = 2P\sin\left(\frac{\theta}{d^2}\right) = 1.8544\frac{P}{d^2} \qquad (1)$$

where P is the indent load in kgf and d is the corner to corner diameter of the indentation in mm and θ is the angle between the indenter face and the vertical (136°/2 = 68°). The depth of the indentation, h, is equal to $d/7$ $(d/2\sqrt{2}\tan\theta)$. Therefore, expressing HV hardness as a function of indentation depth.

$$\mathrm{HV} = \frac{P}{26.42\cdot h^2} \qquad (2)$$

Vickers microhardness is defined as the ratio of applied load to contact area between indenter and sample under load. The SIMM microhardness was determined using the principles outlined in the draft ISO standard for Instrumented Hardness Tests, ISO DIS 14577. The depth sensing hardness HV (SIMM) is defined by P_{max}/A (i.e. $2P/d^2$), where A is the projected area of contact, and this is calculated from

$$\mathrm{HV(SIMM)} = \frac{F}{26.42h_c^2} = 0.93\,\mathrm{HV} \qquad (3)$$

where h_c is the indentation contact depth under load; for relatively high loads, generally above about 2 N for metallic materials, where small discrepancies in the diamond indenter geometry are not a problem. For loads less than about 1 N, small differences in the indenter tip geometry can give rise to significant discrepancies with regard to h_c, compared with what would be expected theoretically, and these discrepancies generally have to be calibrated by experiment. In these circumstances the nominal SIMM hardness values can be significantly larger than the conventional microhardness HV value.

2. SCANNING MICROHARDNESS MEASUREMENTS

Typical SIMM maps from sectioned axisymmetric compression testpieces of 316 stainless steel and Waspaloy are shown in Figures 2 and 3.

The zones associated with constraint by the platens are clearly seen in the high rate tests with no lubrication and compare very well with FE model predictions of temperature and effective strain variation (Figure 4).

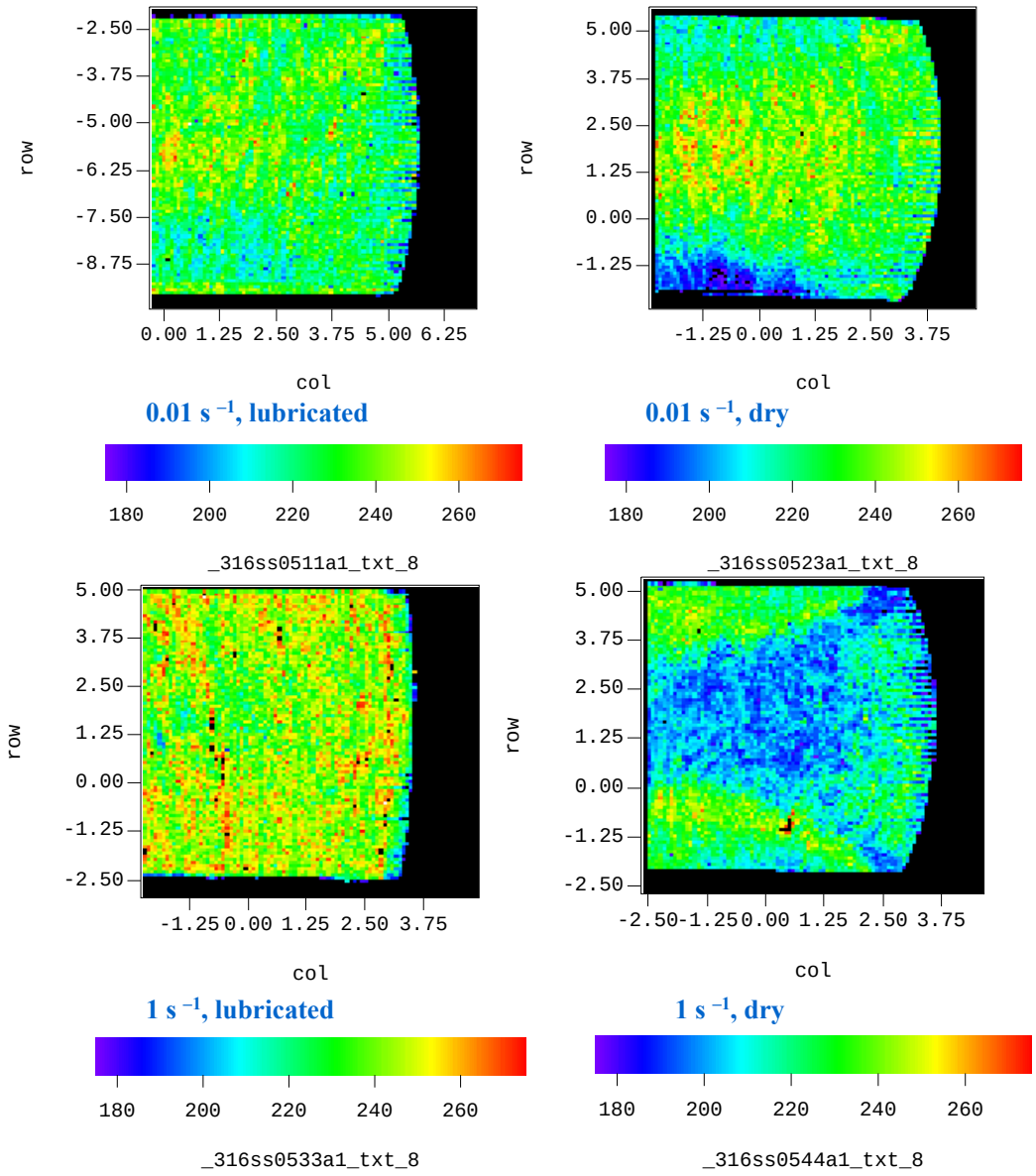

Fig. 2. *SIMM maps for tests on 316 stainless steel at 950°C; 90 × 100 array, 2N, 0.03 mm diameter indents, 0.08 mm spacing.*

The hardness array maps can thus be effectively used to give insight on where to concentrate for the microstructure measurements within the testpieces. Typical line plots of averaged values of hardness are shown in Figure 5 for the 316 stainless steel testpieces.

Similar measurements can be made on the PSC testpieces (Figure 6) and the maps show obvious shear bands corresponding with FE model predictions.

3. EBSD MEASUREMENTS

A typical large map from a PSC testpiece is shown in Figure 7. Currently it is believed that division into strips and/or columns is the most useful way of dealing with these large data sets. The image also illustrates the difficulty of deciding whether to measure by number or by area when faced with a microstructure that combines two populations (recrystallised and unrecrystallised) of significantly different mean size. The issues in the list above are being currently investigated and some preliminary comments are discussed in the following sections:

Effects of step size

A series of maps were acquired at step sizes of 0.5, 1 and 2 μm (or approximately 6, 12 and 20% of the mean grain size) from the same region at the centre of the stainless steel specimen where full recrystallisation was thought to have occurred. The maps are shown in Figure 8. The central 300 × 200 μm area was common to all three maps; but each map extended beyond this region with a different aspect ratio and total size to check that contamination build up in the central region already mapped

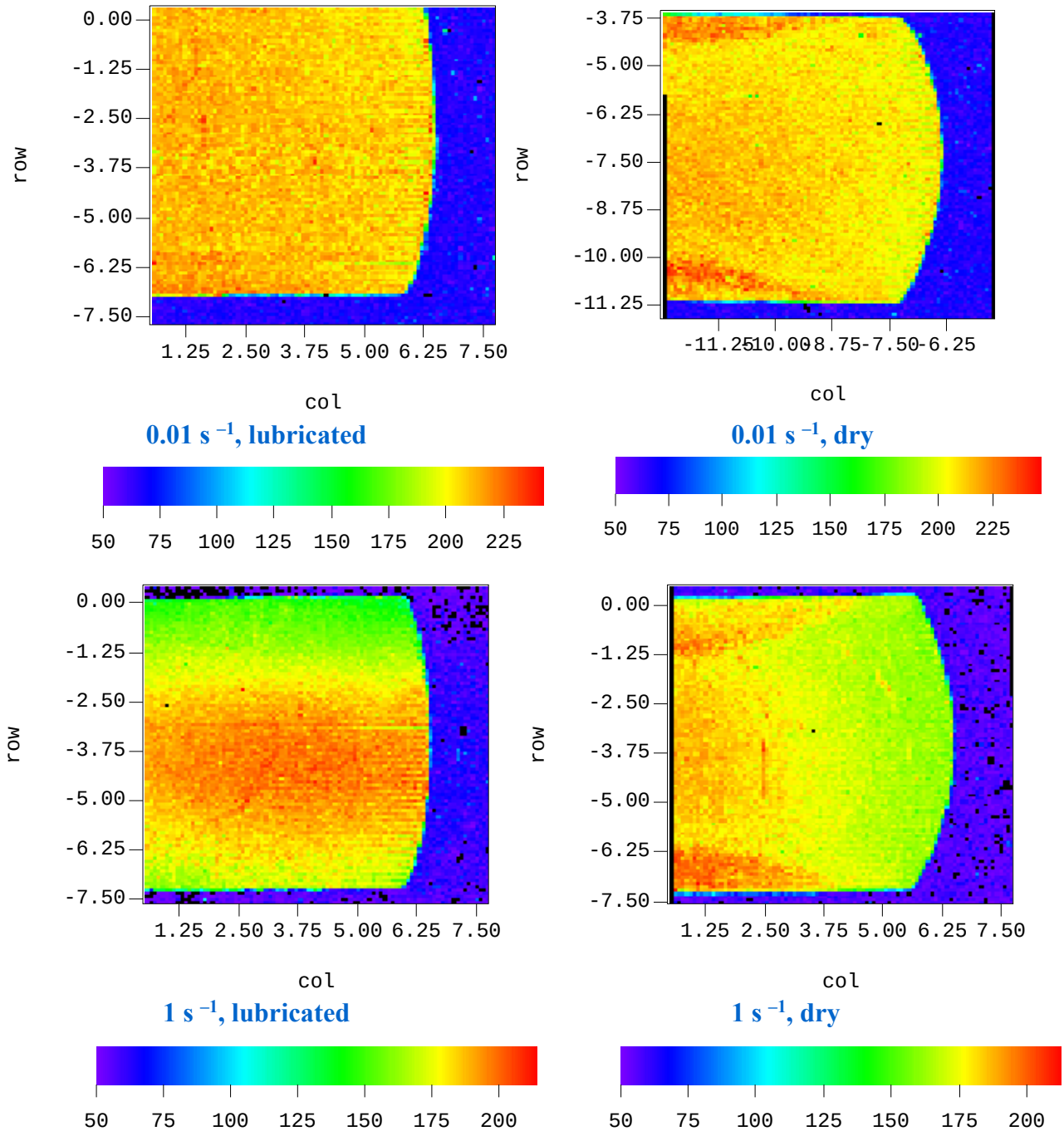

Fig. 3. *SIMM maps for tests on Waspaloy at 1040°C; 90 × 100 array, 2N, 0.03 mm diameter indents, 0.08 mm spacing.*

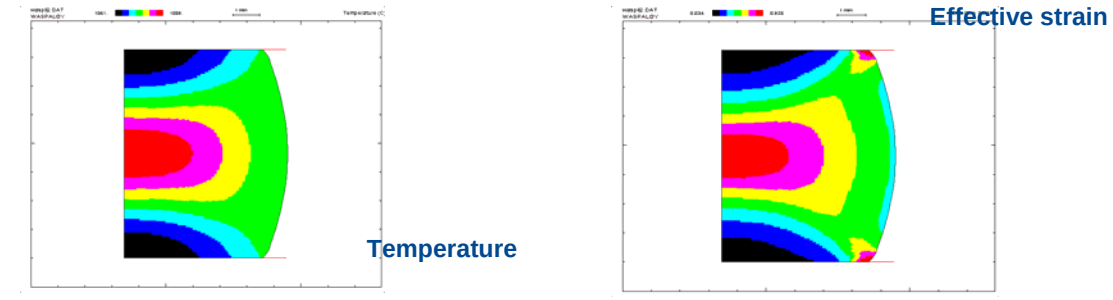

High friction: strain rate 1.0 s^{-1} High friction: strain rate 1.0 s^{-1}

Fig. 4. *FE model predictions of temperature and effective strain variations in high friction, high strain rate tests on Waspaloy.*

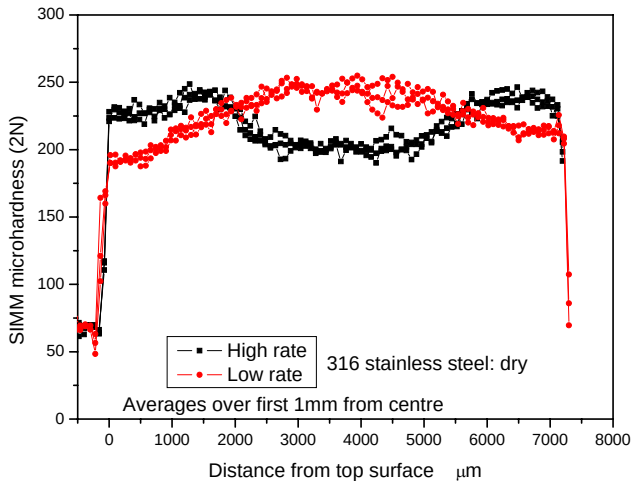

Fig. 5. *Line plots of microhardness for the 316 stainless steel axisymmetric compression testpiece.*

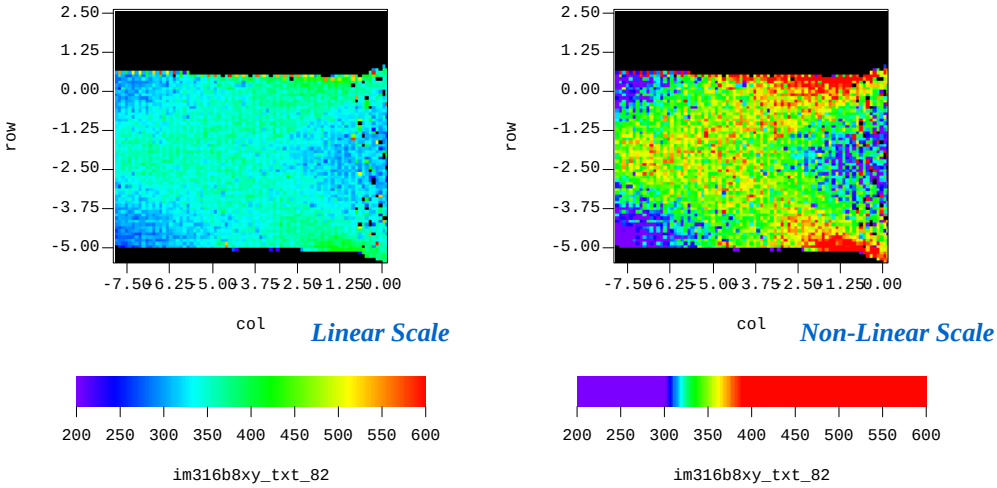

Fig. 6. *Typical hardness map from 316 stainless steel sample deformed dry at 950 ℃ and a strain rate of 0.1 s^{-1}; 80 × 80 array, 2N, 0.03 mm diameter indents, 0.1 mm spacing.*

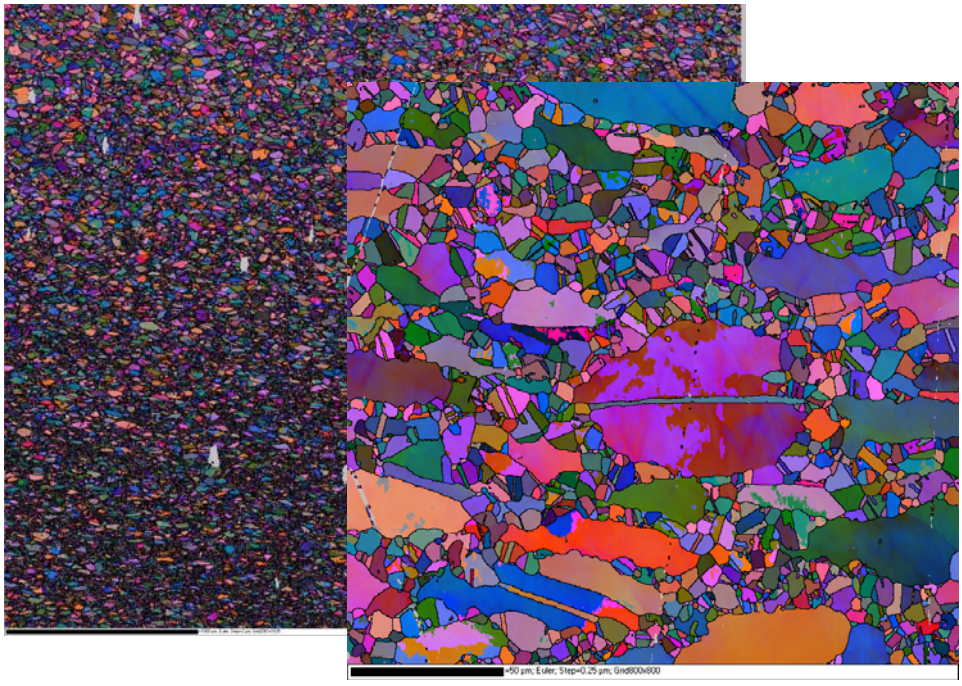

Fig. 7. *Large area EBSD map (inset is high magnification of part of image).*

did not affect the results by degrading EBSD pattern quality. The microstructure was homogeneous across the whole area examined and the small variation in number of grains analysed was taken into account in calculating significance levels. Each step size map was then analysed for grain size using the circle equivalent diameter and linear intercept methods, noting the effect of any noise reduction used. Except where stated, the definition of a grain boundary was set with a lower limit of 10° misorientation and twins were excluded (defined as within 5° of the ideal 60° misorientation about <111>) direction. These definitions are themselves a source of variation, with 10° and 15° both commonly used (Thomas et al., 2005; El Wahabi et al., 2005; Dingley, 2004). Circle equivalent grain size d_{ceq} distributions showed that altering the step size had an effect on the lower end of the size distribution below about 5 μm. The 2 μm step size is too large a spacing for the small grains, while the 0.5 μm step size produced a distribution which approximated much more closely to a typically shaped grain size distribution.

Effects of Noise Reduction

The large number of data points at the single pixel level has a very significant effect on mean values. It is common for these single pixels (commonly called "wildspikes") to be removed as noise. Groups of up to 5 pixels (Bastos et al., 2006) are sometimes removed to eliminate possible spurious results. Also commonly employed is the technique of filling

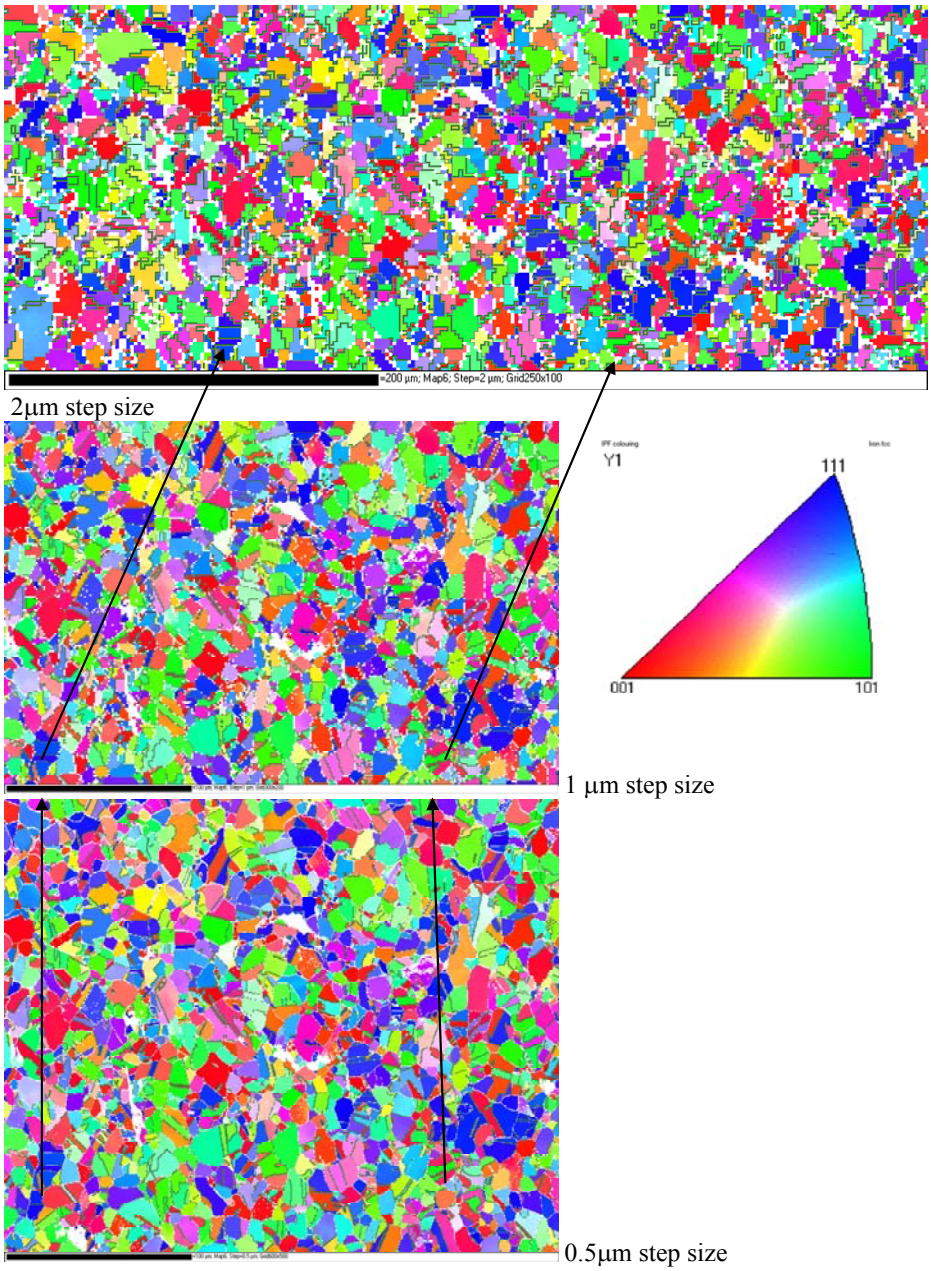

Fig. 8. *Raw EBSD maps (no noise reduction) of overlapping areas, made at the three different step sizes indicated. Grains coloured according to the Inverse Pole Figure colouring shown. Identical grains shown arrowed.*

in non-indexed pixels with a copy of neighbouring pixel orientation, where the number of indexed neighbouring pixels is set to a minimum number (usually six). To explore these factors of wildspikes and non indexing, the 0.5µm step size data was edited using various combinations of the above noise reduction routines. Even though 90% of the original map was indexed it was possible to alter the d_{ceq} grain size significantly by the noise reduction. Removal of the wildspikes had a larger effect on the geometric mean than on the arithmetic mean, but for the latter infilling had just as large an effect as the wildspike removal. With the noise reduction routine filling non-indexed pixels having 6 or more adjacent indexed pixels, the infilling of grain boundaries around larger grains was the dominant effect on the arithmetic mean. When the same operations were carried out on the 2 µm step size the effect of removing wildspikes had a greater influence than the growth into unfilled regions, as might be expected since each wildspike is a greater proportion of the actual grain size and non-indexing at grain boundaries is much less frequent. Removing wildspikes and growing into non-indexed regions with 6 neighbours produced an increase of 26% in measured grain size compared with the 15% increase for the same operation at 0.5 µm step size. Thus the choice of the appropriate step size becomes even more important if the acquired data is noisy and noise reduction routines are required.

Linear intercept measurement of grain size

Linear intercept measurements were made with the EBSD software, inserting measurement lines approximately 20 µm apart, horizontally (in line with the applied strain direction) across the images shown in Figure 8. The software determines the positions of the intercepts in the same way that it defines grain boundaries. Typically 350 values were obtained by this method, compared with an average of 850 using the same dataset for grain size area. Results are shown in Figure 9 where the cumulative frequency curves for the linear intercept d_{lin} measurements (at each step size) are plotted with the data

for circle equivalent diameter d_{ceq}. The different step sizes produce some divergence in linear intercept data at small values, but the reduced number of these small values means the results for d_{lin} are less sensitive to step size and 95% confidence intervals are very slightly smaller at ± 7%. The linear intercept method is less sensitive to step size because only a fraction of the smallest grains are sampled. For example, the percentage increase in arithmetic mean grain size d_{lin} between the 0.5 μm and 1 μm step maps is half that of the increase in arithmetic mean d_{ceq} for the same maps

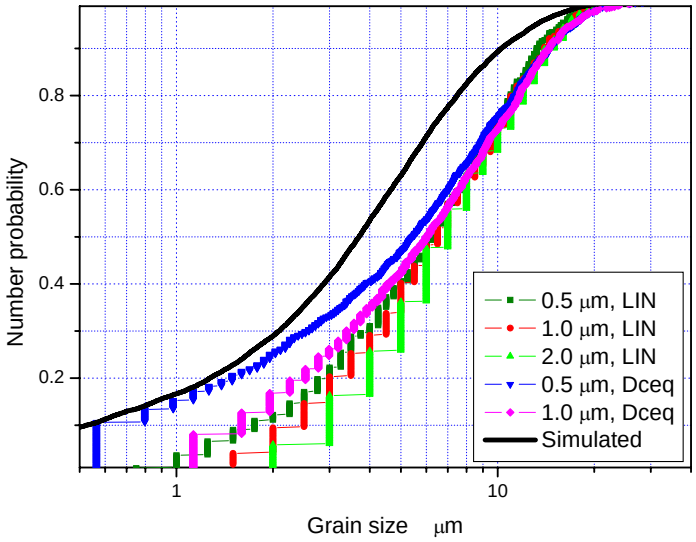

Fig. 9. *Cumulative number probability plot of grain size distribution measured by linear intercept (LIN), from the maps with step sizes of 0.5, 1 and 2 μm, compared with circle equivalent diameter size (Dceq) data and simulated intercept size distribution for the tetrakaidecahedron model.*

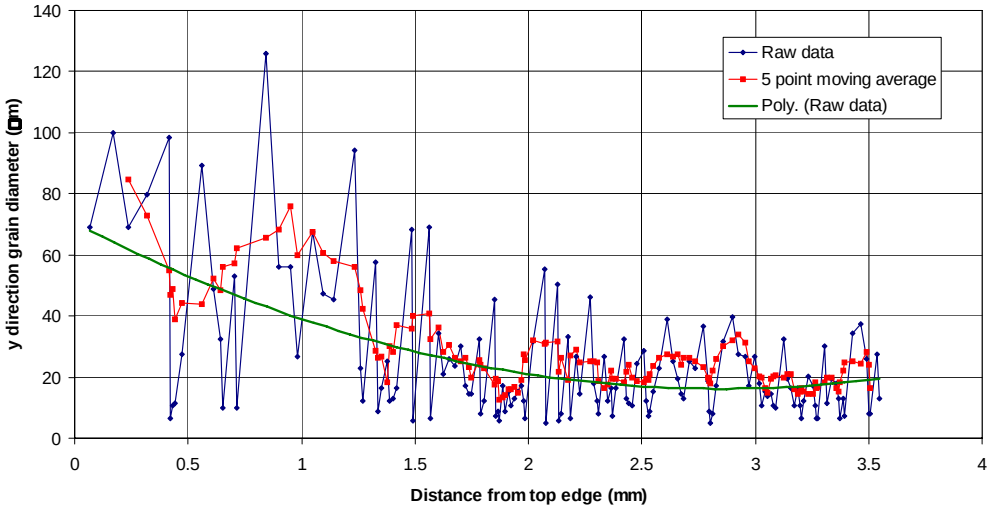

Fig. 10. *Grain size heterogeneity in strip through Waspaloy compression testpiece.*

Linear intercept measurements were made by light optical microscope in the same region of the sample, after etching. They were also compared with measurements by University of Wales, Swansea on a separate but identically processed sample. Digital images of the etched samples were acquired with a 20× objective lens and two operators then measured intercepts on sets of lines 25 μm apart, giving approximately 250 measurements. Twin boundaries were ignored. Operator variability was clearly seen in the results but with 95% confidence intervals of > ±10% they were approximately equivalent. However, there was a 25% increase over the EBSD measurements in the same orientation. Possible reasons for this include failure of the etch to reveal all grain boundaries, and a failure to resolve all the small grains identified by EBSD. These effects would both tend to cause overestimates of grain size by the optical method, although they would to some extent be counteracted by the mistaken inclusion of some twin boundaries.

Analysis of grain size variation over large areas

Figure 1 shows an EBSD orientation map for a Ni superalloy (Waspaloy) with inverse pole figure colouring. The map was acquired with a 1 μm step size from the centre line of an axial cross section of a cylindrical axisymmetric compression. The sample was produced with relatively high friction between sample and plattens, resulting in a region of large unrecrystallised grains close to the surface while the inner region consists of many smaller recrystallised grains. Noise reduction was performed by removing wildspikes of single pixels and then growing into non indexed pixels with 4 neighbouring pixels of the same orientation. Further analysis was carried out by removing all grains of 3 pixels ($d_{ceq} \approx 2$ μm). Figure 10 shows the variation of d_{ceq} (prior to the removal of 3 pixel grains) with distance from the top surface by plotting the size of each grain (ignoring those impinging on map edges) against its distance from the top surface irre-

spective of its lateral position. Superimposed on the raw data is the moving average calculated over 50 grains which shows the trend in grain size more clearly and also emphasises the variation in the distribution from the edge to the centre of the sample. These effects can be reduced if the moving average is taken over a smaller number of grains. As is to be expected plots become noisier as the number of grains averaged over are reduced, but the maxima are particularly accentuated near the surface where there are fewer large grains, so the overall change in size appears larger.

The EBSD measurements described above were compared with those obtained from two samples processed identically at the same time and assessed in a similar section by EBSD (at Sheffield University) with a linear intercept measurement on a 4 μm step map, and by optical linear intercept (at Swansea University). Despite the coarse 4 μm step size the correspondence of the average grain size by EBSD in the centre of the sample was very good. The coarser step size did not increase grain size towards the surface as much as the finer step size, reflecting partly the sample variation but mostly a poor level of indexing in the region closest to the surface.

4. SUMMARY

The assessment of grain size across a section of a hot deformed sample illustrates that the choice of step size and of the range over which averaging is applied are very important when changes in grain size are being assessed over large areas. For the recrystallised 316L stainless steel specimen, increasing the EBSD step size from 5% to 20% of the approximate mean grain size results in a change in calculated arithmetic mean grain size of >15%, based on a circle equivalent diameter value. The grain size distribution did not appear to be log-normal, having a large number of very small grains, and thus the geometric mean is no more appropriate than the arithmetic mean for quantifying the grain size of the microstructures examined here. The choice of noise reduction methods can also lead to changes in calculated mean grain size greater in magnitude than that produced by the different step sizes. Careful consideration needs to be given to the size and location of pixel blocks removed as noise, since a theoretical examination suggests that a 2-D section should result in many very small grain cross sections. EBSD linear intercept measurements appear slightly less sensitive to step size and noise reduction than the use of circle equivalent diameters and results in a larger measure of mean grain size because fewer of the very small grains are sampled. Optical linear intercept measurements produced measurements of grain size larger than EBSD measurements of the same sample because fewer small grains were resolved by etching and the use of the optical technique and some grain boundaries were simply missed by eye. Scanning microhardness maps provide useful insight on microstructural heterogeneity, enabling more focused studies to be performed of microstructural variations. A "Good Practice" document is planned for 2008 to capture recommendations on how and where best to make microstructure measurements in deformed testpieces.

ACKNOWLEDGEMENTS

This work was supported by the UK Department of Trade and Industry Materials Measurement Programmes. Materials for the study were provided by members of various DTI Measurement Programme Industrial Advisory Groups. Colleagues at the University of Wales (Swansea) are thanked for their contributions including optical measurements of microstructure and complementary modelling studies of deformed testpieces.

REFERENCES

Bastos, A., Zaefferer, S., Raabe, D., Schuh, C., 2006, Characterization of the microstructure and texture of nanostructured electrodeposited NiCo using electron backscatter diffraction (EBSD), *Acta. Mater*., 54, 2451-2462.

Dingley, D., 2004 Progressive steps in the development of electron microscopy and orientation imaging microscopy, *J. Microscopy*, 213, 214-224.

El Wahabi, M., Gavard, L., Cabrera, J.M.,. Prado, J.M., Montheillet, F., 2005, EBSD study of purity effects during hot working in austenitic stainless steels, *Mater. Sci. Eng. A*, 393, 83-90.

Humphreys, F.J., 2001, Grain and subgrain characterisation by electron backscattered diffraction, *J. Mater. Sci*., 36, 3833-3854.

Loveday, M.S., Mahon, G.J., Roebuck, B, Lacey, A.J., Palmiere, E.J., Sellars, C.M.,van der Winden, M.R., 2006, Measuring Flow Stress in Hot Plane Strain Compression Tests. (*NPL Good Practice Guide No.27, Revised Summer 2002*) Materials at High Temperatures, 23(2), 85-118.

Randle, V., 2003, *Microtexture determination and its applications*, 2nd edn. London, Institute of Materials/Maney.

Roebuck, B., Lord, J.D., Brooks, M., Loveday, M.S., Sellars, C.M., Evans, R.W., 2006, Measuring Flow Stress in Hot Axisymmetric Compression Tests. (*NPL Good Practice Guide No.3, Revised Summer 2002*) Materials at High Temperatures, 23 (2), 59-83.

Roebuck, B., Loveday, M.S., Chastel, Y., Fiorucci, G., Dal Negro, T., 2006, High Temperature Solid Torsion Tests. (*NPL Good Practice Guide No.58, May 2003*) Materials at High Temperatures, 23 (2), 119-144.

Roebuck, B., Stewart, M., Morrell, R., Gee, M.G., Plint, G., 2001, Mapping Hardness Using Automated Depth Sensing Process, *Surface Engineering*, 17, 447-449.

Thomas, M.J., Wynne, B.P., Rainforth, W.M., 2005, An alternative method to separate and analyse the microtextures and microstructures of primary alpha and transformed beta grains in near-α titanium Timetal 834, *Mater. Characterization*, 55, 388-394.

BADANIE MIKROSTRUKTURY W OSIOWOSYMETRYCZNYCH I PŁASKICH PRÓBKACH ODKSZTAŁCANYCH W WYSOKIEJ TEMPERATURZE

Streszczenie

Dobra baza pomiarowa ma kluczowe znaczenie dla dostarczenia danych dla rozwoju modeli numerycznych procesów, które stworzą lepsze możliwości sterowania tymi procesami w warunkach produkcyjnych. Konsorcjum zajmujące się w Wielkiej Brytanii organizacją badań technologicznych opracowało standardy (good practice guides) dla prób plastometrycznych prowadzonych w wysokich temperaturach, takich jak osiowosymetryczne ściskanie, ściskanie próbek płaskich i skręcanie. Aby kontynuować tą aktywność postawiono sobie nowy cel, jakim jest opracowanie standardu dla pomiarów lokalnej mikrostruktury w rozumieniu wielkości ziarna, wielkości różnych faz oraz kształtu, rozkładu i ułamka objętości nowej fazy (lub ułamka objętości zrekrystalizowanej). Problemy pomiarów są rozpatrywane mając na uwadze nowe metody charakteryzacji struktury, na przykład pomiar orientacji i twardości, przede wszystkim w odniesieniu do analizowanych prób plastometrycznych.

Received: June 11, 2007
Received in a revised form: November 30, 2007
Accepted: December 3, 2007